NCAR

EULAG: a computational model for multi-scale flows, an overview

Piotr K Smolarkiewicz*,

Geophysical turbulence; scales of motion $\mathcal{O}(10^7)$, $\mathcal{O}(10^4)$, and $\mathcal{O}(10^{-2})$ m.

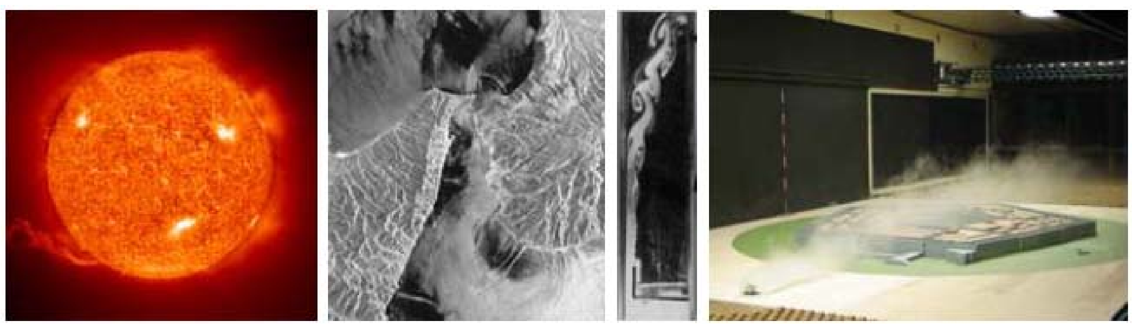

A range of applications

*National Center for Atmospheric Research, Boulder, Colorado, U.S.A.

EULAG ≡ *EUlerian/semi-LAGrangian numerical model for fluids*

NCAR

Theoretical Features

Two optional modes for integrating fluid PDEs:

- Eulerian --- control-volume wise integral
- Lagrangian --- trajectory wise integral

Numerical algorithms:

- Nonoscillatory Forward-in-Time (NFT) for the governing PDEs
- Preconditioned non-symmetric Krylov-subspace elliptic solver GCR(k)
- Generalized time-dependent curvilinear coordinates for grid adaptivity

Optional fluid equations (nonhydrostatic):

- Anelastic (Ogura-Phillips, Lipps-Hemler, Bacmeister-Schoeberl, Durran)
- Compressible/incompressible Boussinesq,
- Incompressible Euler/Navier-Stokes'
- Fully compressible Euler equations for high-speed flows

Note: not all options are user friendly !

Available strategies for simulating turbulent dynamics:

- Direct numerical simulation (DNS)
- Large-eddy simulation, explicit and implicit (LES, ILES)

Multi-time scale evolution of a meso-scale orographic flow (Smolarkiewicz & Szmelter, 2008, JCP, in press)

NCAR

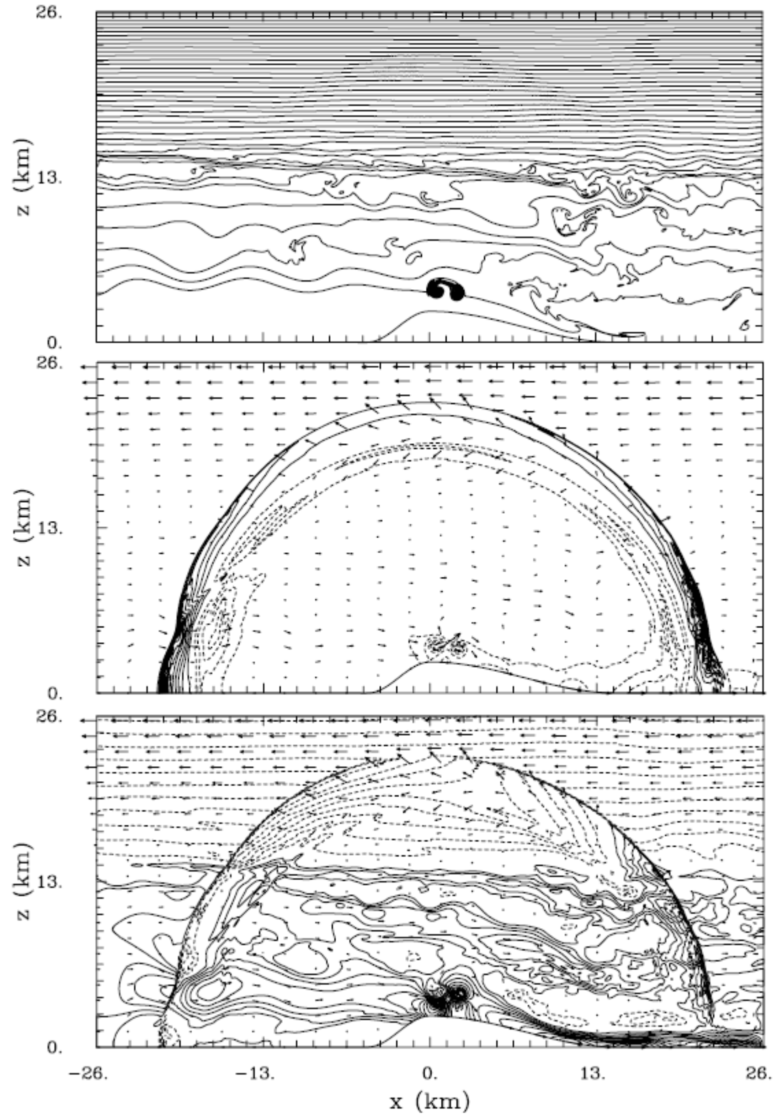

A Brief History

- Early 1980’s (plus), development of MPDATA
- Late 1980’s/early 1990’s, semi-Lagrangian advection and its extension on fluid systems
- Early 1990’s, congruence of SL and EU and formulating GCR(k) pressure solver
- Mid 1990’s, time-dependent lower boundary, extension to spheres (EulaS), parallelization
- Late 1990’s/early 2000’s, unification of EULAG and EULAS
- 2000’s , generalized coordinates and applications, unstructured meshes

Tenets of EULAG:

Simplicity: a compact mathematical/numerical formulation

Generality: interdisciplinary multi-physics applications

Reliability: consistent stability and accuracy across a range
of Froude, Mach, Reynolds, Peclet (etc.) numbers

Mathematical Formulation

NCAR

Multidimensional positive definite advection transport algorithm (MPDATA):

$$\frac{\partial \phi}{\partial t} = -\nabla \bullet (\mathbf{V}\phi) \ , \qquad \phi_i^{n+1} = \phi_i^n - \frac{\delta t}{\mathcal{V}_i} \sum_{j=1}^{l(i)} F_j^{\perp} S_j$$

$$F_j^{\perp}(\phi_i, \phi_j, V_j^{\perp}) = [V_j^{\perp}]^+ \phi_i + [V_j^{\perp}]^- \phi_j \ , \qquad [V]^+ \equiv 0.5(V + |V|) \ \ , \ \ [V]^- \equiv 0.5(V - |V|) \ ,$$

$$\phi_i^{(k)} = \phi_i^{(k-1)} - \frac{\delta t}{\mathcal{V}_i} \sum_{j=1}^{l(i)} F_j^{\perp} \left(\phi_i^{(k-1)}, \phi_j^{(k-1)}, V_j^{\perp,(k)} \right) S_j$$

with $k = 1, .., IORD$ such that

$$\phi^{(0)} \equiv \phi^n \ \ ; \ \ \phi^{(IORD)} \equiv \phi^{n+1}$$

$$V^{\perp,(k+1)} = V^{\perp} \left(\mathbf{V}^{(k)}, \phi^{(k)}, \nabla \phi^{(k)} \right) \ \ ; \ \ V_j^{\perp,(1)} \equiv V^{\perp}\Big|_j^{n+1/2}$$

$$V^{\perp}\Big|_{s_j}^{(k+1)} = \Bigg\{ \ 0.5|V^{\perp}| \left(\frac{1}{|\phi|} \frac{\partial |\phi|}{\partial r} \right) (r_j - r_i) \ - 0.5 V^{\perp} \left(\frac{1}{|\phi|} \frac{\partial |\phi|}{\partial r} \right) (r_i - 2r_{s_j} + r_j)$$

$$- 0.5 \delta t V^{\perp} \left(\mathbf{V} \bullet \frac{1}{|\phi|} \nabla |\phi| \right) - 0.5 \delta t V^{\perp} (\nabla \bullet \mathbf{V}) \Bigg\}\Bigg|_{s_j}^{(k)}$$

Abstract archetype equation for fluids, e.g.,

Eulerian conservation law | *Lagrangian* evolution equation

$$\frac{\partial \rho^* \psi}{\partial \bar{t}} + \overline{\nabla} \bullet (\rho^* \overline{\mathbf{v}}^* \psi) = \rho^* R \qquad \Leftrightarrow \qquad \frac{d\psi}{d\bar{t}} = R$$

$\psi \equiv v^j \text{ or } \theta'$ Kinematic or thermodynamic variables, R the associated rhs

Numerical design

NCAR

Either form (Eulerian/semi-Lagrangian) is approximated to second-order using a template algorithm:

$$\boxed{\psi_{\mathbf{i}}^{n+1} = LE_{\mathbf{i}}(\psi^n + 0.5\Delta t R^n) + 0.5\Delta t R_{\mathbf{i}}^{n+1}}$$

where $\psi_{\mathbf{i}}^{n+1}$ is the solution sought at the grid point $(\overline{t}^{n+1}, \overline{\mathbf{x}}_{\mathbf{i}})$

LE a two-time-level either advective semi-Lagrangian or flux-form Eulerian NFT transport operator (Sm. & Pudykiewicz, *JAS*,1992; Sm. & Margolin, *MWR* 1993).

Numerical design

NCAR

Motivation for Lagrangian integrals

$$\boxed{\frac{d\Psi}{dt} = R}$$

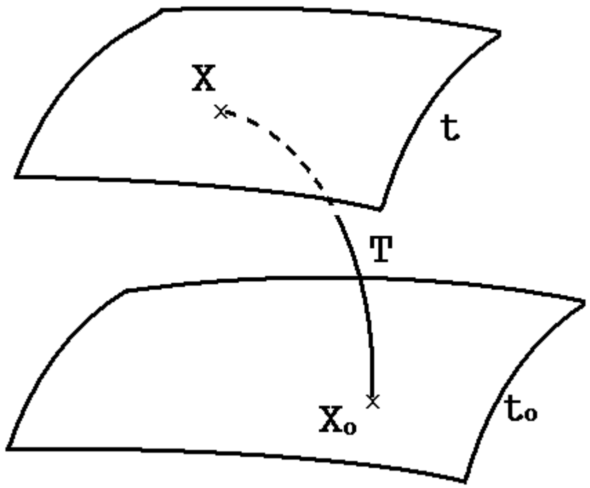

$$\Psi(\mathbf{x}, t) = \Psi(\mathbf{x}_o, t_o) + \int_T R d\tau$$

$$\Psi_{\mathbf{i}}^{n+1} = \Psi_o + 0.5\delta t(R_{\mathbf{i}}^{n+1} + R_o) + \delta t\mathcal{O}(\delta t^2)$$

$$\Psi_{\mathbf{i}}^{n+1} = (\Psi + 0.5\delta t R)_o + 0.5\delta t R_{\mathbf{i}}^{n+1} + \mathcal{HOT}$$

$$\boxed{\Psi_i^{n+1} = LE_i(\Psi^n + 0.5\Delta t R^n) + 0.5\Delta t R_i^{n+1}}$$

Numerical design

NCAR

Motivation for Eulerian integrals

$$\boxed{\frac{\partial G\Psi}{\partial t} + \nabla \cdot (\mathbf{v}\Psi) = GR}$$

Forward in time temporal discretization

$$\frac{G^{n+1}\Psi^{n+1} - G^n\Psi^n}{\delta t} + \nabla \cdot (\mathbf{v}^{n+1/2}\Psi^n) = (GR)^{n+1/2}$$

Second order Taylor sum expansion about t=nΔt

$$\frac{\partial G\Psi}{\partial t} + \nabla \cdot (\mathbf{v}\Psi) \;=\; GR - \nabla \cdot \left[\frac{\delta t}{2} G^{-1}\mathbf{v}(\mathbf{v}\cdot\nabla\Psi) + \frac{\delta t}{2} G^{-1}\left(\frac{\partial G}{\partial t} + \nabla\cdot\mathbf{v}\right)\mathbf{v}\Psi\right] + \;\nabla \cdot \left(\frac{\delta t}{2}\mathbf{v}R\right) + \mathcal{O}(\delta t^2)$$

Compensating first error term on the rhs is a responsibility of an FT advection scheme (e.g. MPDATA). The second error term depends on the implementation of an FT scheme

$$\boxed{\Psi_i^{n+1} = LE_i(\Psi^n + 0.5\Delta t R^n) + 0.5\Delta t R_i^{n+1}}$$

Numerical design

NCAR

All principal forcings are assumed to be unknown at *n*+1

$$\psi_{\mathbf{i}}^{n+1} = LE_{\mathbf{i}}(\psi^n + 0.5\Delta t R^n) + 0.5\Delta t R_{\mathbf{i}}^{n+1}$$

$\Rightarrow$ system implicit with respect to all dependent variables.

On grids co-located with respect to all prognostic variables, it can be inverted algebraically to produce an elliptic equation for pressure

$$\left\{\frac{\Delta t}{\rho^*}\overline{\nabla}\cdot\rho^*\widetilde{\mathbf{G}}^T\left[\widehat{\widehat{\mathbf{v}}} - (\mathbf{I} - 0.5\Delta t\widehat{\mathbf{R}})^{-1}\widetilde{\mathbf{G}}(\overline{\nabla}\pi'')\right]\right\}_{\mathbf{i}} = 0$$

solenoidal velocity $\overline{\mathbf{v}}^s \equiv \overline{\mathbf{v}}^* - \dfrac{\partial\overline{\mathbf{x}}}{\partial t}$ *contravariant velocity* $\overline{\mathbf{v}}^* \equiv d\overline{\mathbf{x}}/d\overline{t} \equiv \dot{\overline{\mathbf{x}}}$

$$\widetilde{\mathbf{G}}^T[\widehat{\widehat{\mathbf{v}}} - (\mathbf{I} - 0.5\Delta t\widehat{\mathbf{R}})^{-1}\widetilde{\mathbf{G}}(\overline{\nabla}\pi'')] \equiv \overline{\mathbf{v}}^s$$

Boundary conditions on π'' Imposed on $\overline{\mathbf{v}}^s \bullet \mathbf{n}$ subject to the integrability condition

$$\int_{\partial\Omega}\rho^*\overline{\mathbf{v}}^s \bullet \mathbf{n}\,d\sigma = 0$$

Boundary value problem is solved using nonsymmetric Krylov subspace solver
- a preconditioned generalized conjugate residual GCR(*k*) algorithm
(Smolarkiewicz and Margolin, 1994; Smolarkiewicz et al., 2004)

Dynamic grid adaptivity

NCAR

Prusa & Sm., *JCP* 2003; Wedi & Sm., *JCP* 2004, Sm. & Prusa, *IJNMF* 2005

- A generalized mathematical framework for the implementation of deformable coordinates in a generic Eulerian/semi-Lagrangian format of nonoscillatory-forward-in-time (NFT) schemes
- Technical apparatus of the Riemannian Geometry must be applied judiciously, in order to arrive at an effective numerical model.

Diffeomorphic mapping

$$(\overline{t}, \overline{x}, \overline{y}, \overline{z}) \equiv (\ t,\ E(t,x,y),\ D(t,x,y),\ C(t,x,y,z)\ )$$

(t,x,y,z) does not have to be Cartesian!

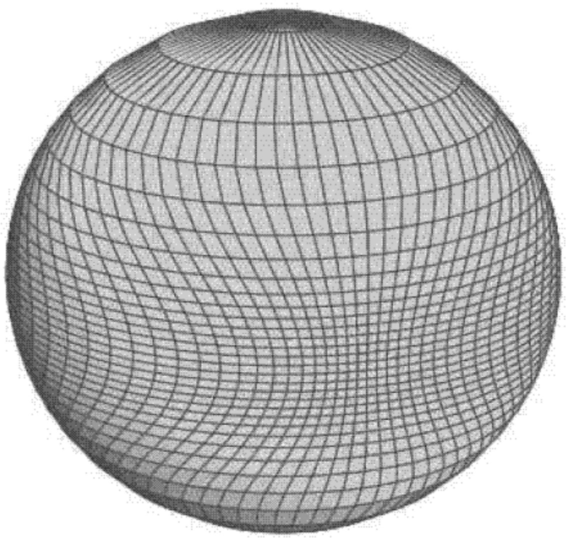

Example: Continuous global mesh transformation

Boundary-fitted mappings; e.g., LES of a moist mesoscale valley flow (Sm. & Prusa, *IJNMF* 2005)

NCAR

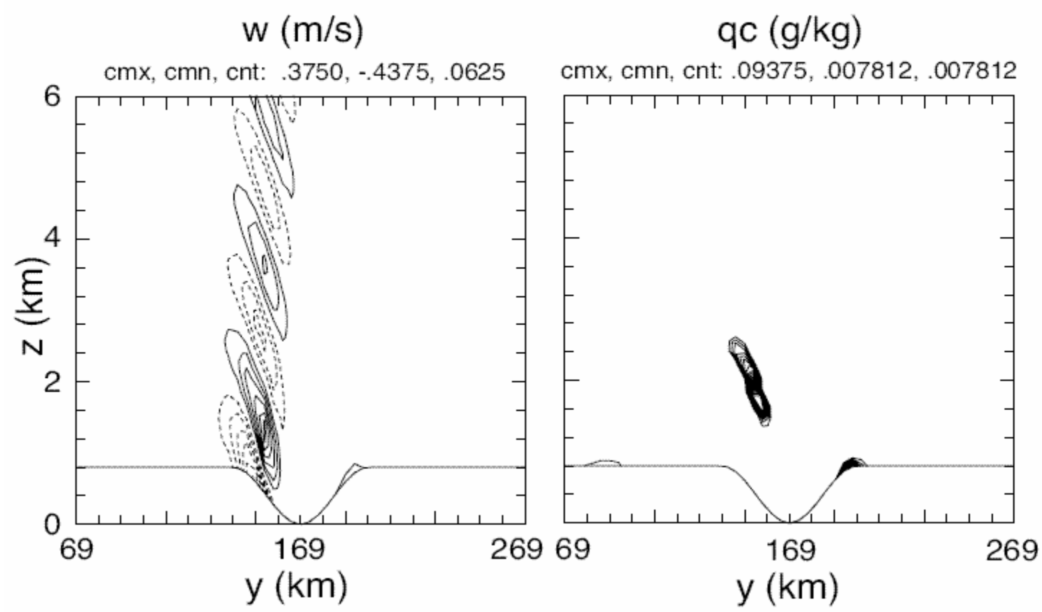

Vertical velocity (left panel) and cloud water mixing ratio (right panel) in the yz cross section at x=120 km

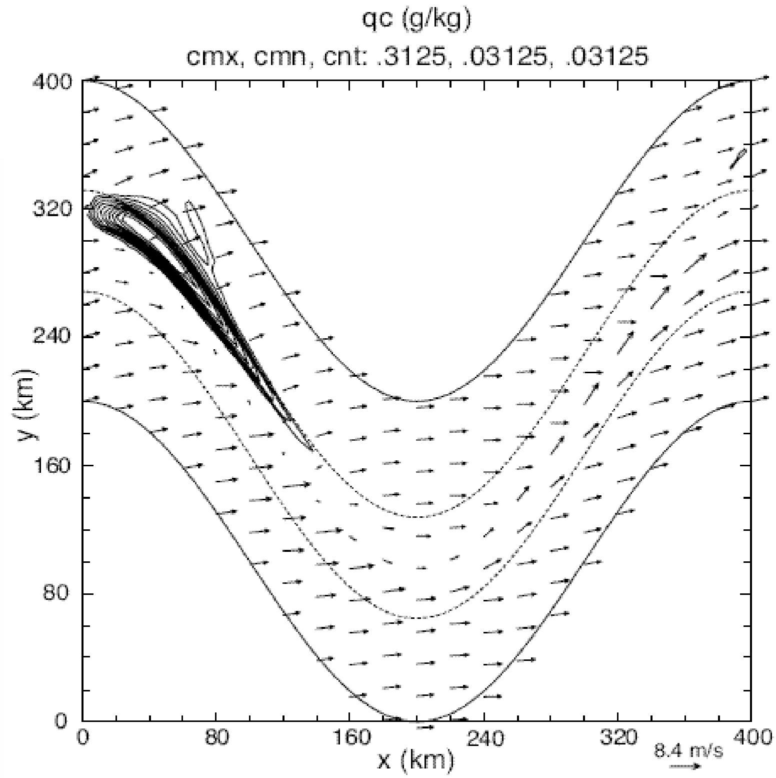

Cloud-water mixing ratio at bottom surface of the model

Boundary-adaptive mappings (Wedi & Sm., *JCP*, 2004)

NCAR

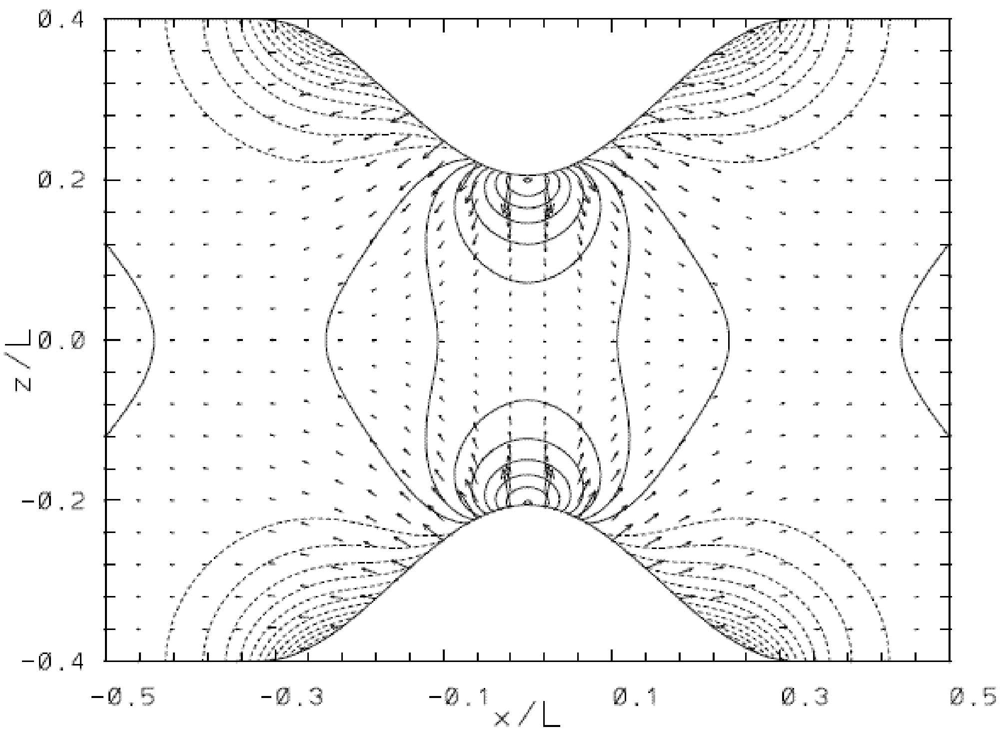

3D potential flow past undulating boundaries

Sem-Lagrangian option; Courant number ~5.

fi eld	Max $\|.\|$	Average	Standard deviation
$\Delta t \omega^1$	$6.99 \cdot 10^{-2}$	$-4.87 \cdot 10^{-18}$	$1.90 \cdot 10^{-3}$
$\Delta t \omega^2$	$6.98 \cdot 10^{-2}$	$-3.19 \cdot 10^{-17}$	$1.90 \cdot 10^{-3}$
$\Delta t \omega^3$	$7.62 \cdot 10^{-3}$	$2.20 \cdot 10^{-18}$	$1.71 \cdot 10^{-4}$
$\Delta t \Delta x \nabla \bullet \boldsymbol{\omega}^s$	$3.73 \cdot 10^{-3}$	$2.12 \cdot 10^{-17}$	$4.81 \cdot 10^{-5}$

Vorticity errors in potential-flow simulation

Boundary fitting mappings (Wedi & Sm., *JCP*, 2004)

NCAR

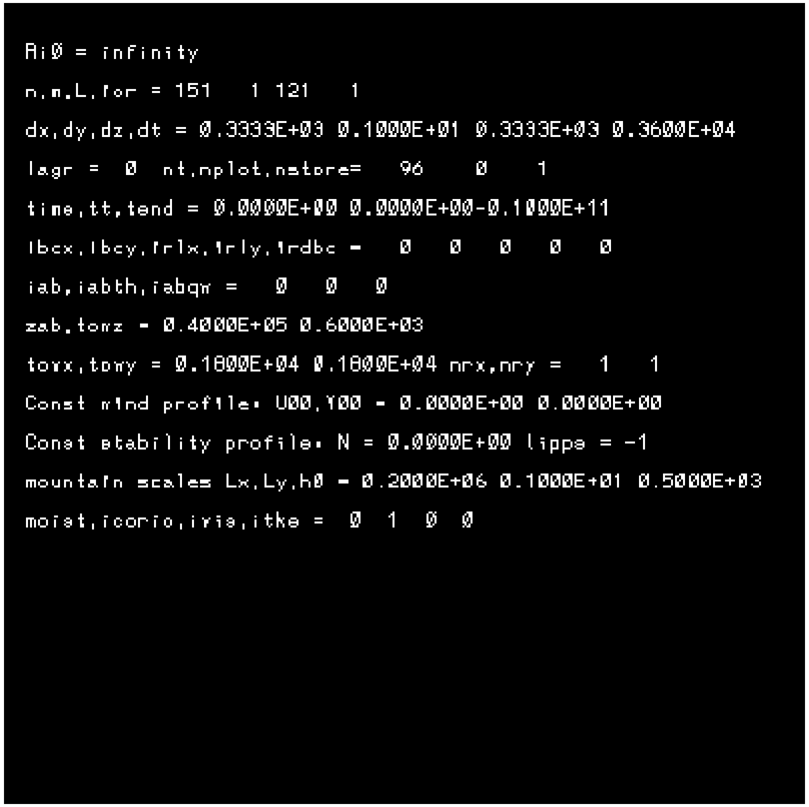

3D potential flow past undulating boundaries

Sem-Lagrangian option; Courant number ~5.

fi eld	Max $\|.\|$	Average	Standard deviation
$\Delta t\omega^1$	$6.99\cdot10^{-2}$	$-4.87\cdot10^{-18}$	$1.90\cdot10^{-3}$
$\Delta t\omega^2$	$6.98\cdot10^{-2}$	$-3.19\cdot10^{-17}$	$1.90\cdot10^{-3}$
$\Delta t\omega^3$	$7.62\cdot10^{-3}$	$2.20\cdot10^{-18}$	$1.71\cdot10^{-4}$
$\Delta t\Delta x\nabla\bullet\boldsymbol{\omega}^s$	$3.73\cdot10^{-3}$	$2.12\cdot10^{-17}$	$4.81\cdot10^{-5}$

Vorticity errors in potential-flow simulation

NCAR

Example: free-surface "real" water flow (Wedi & Sm., *JCP*,2004)

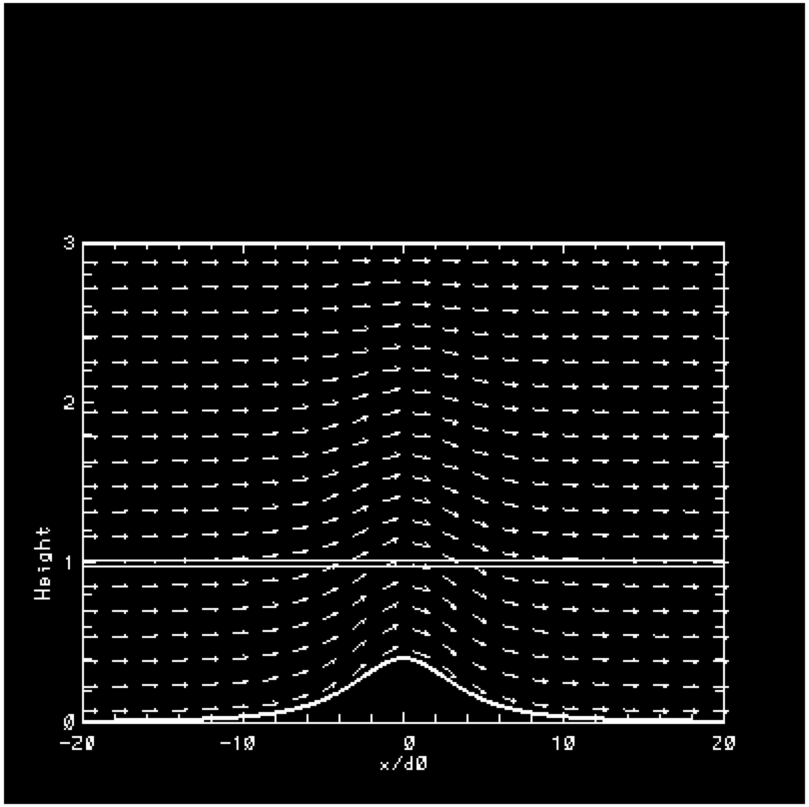

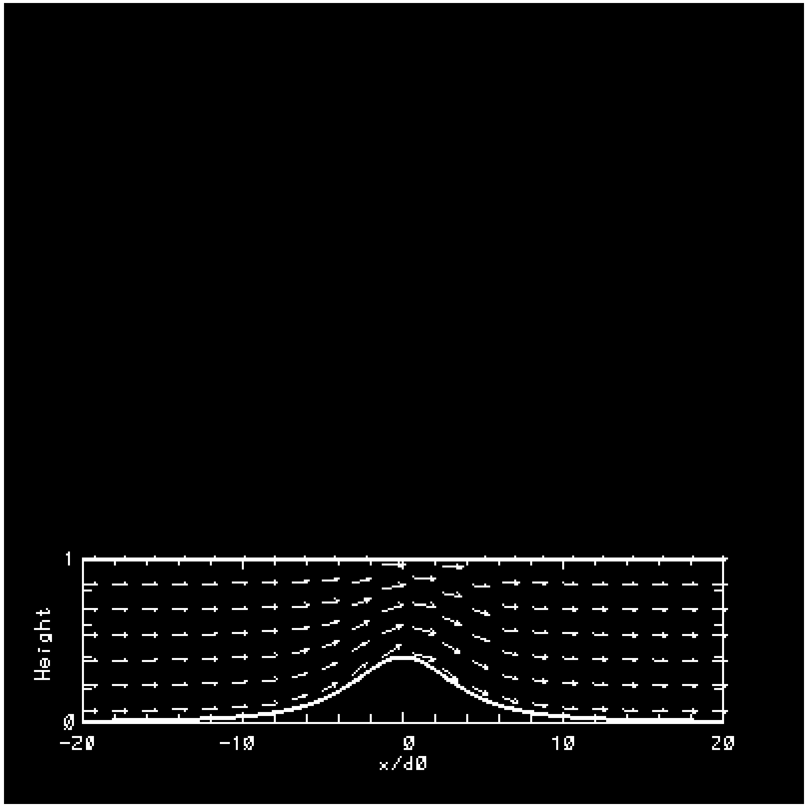

Targeted flow features (Prusa & Sm., *JCP*, 2003)

NCAR

The mesh evolution is postulated via 'mesh-continuity" equation: $\frac{\partial \delta_x}{\partial \bar{t}} + \frac{\partial U \delta_x}{\partial \bar{x}} = 0$

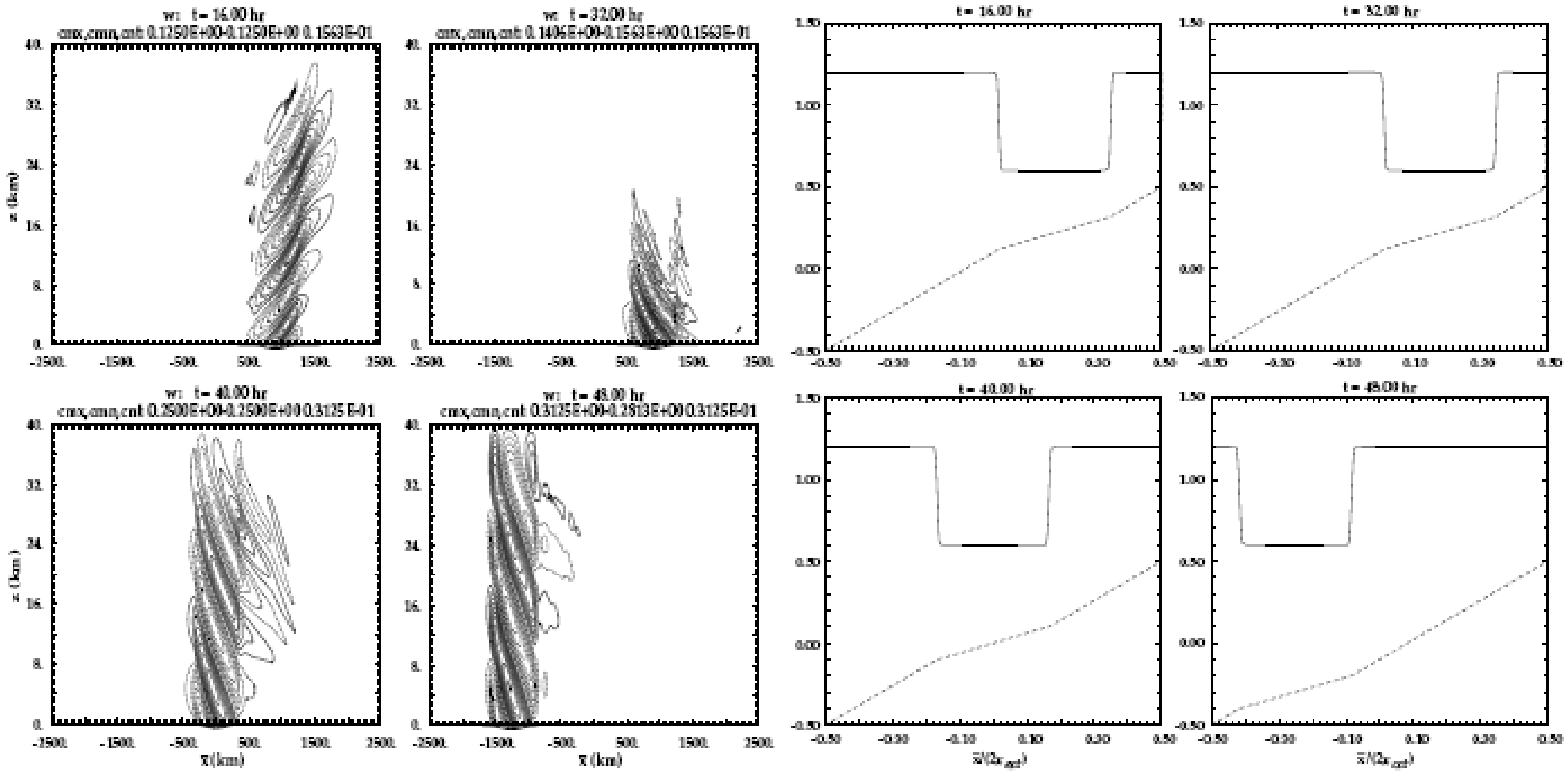

Figure 9: Traveling inertia-gravity wave packet, Prusa & Sm., JCP 2003; grid stretching factor $\delta_x/\Delta\bar{x}$ (solid line) and physical coordinate $x(\bar{t},\bar{x})$.

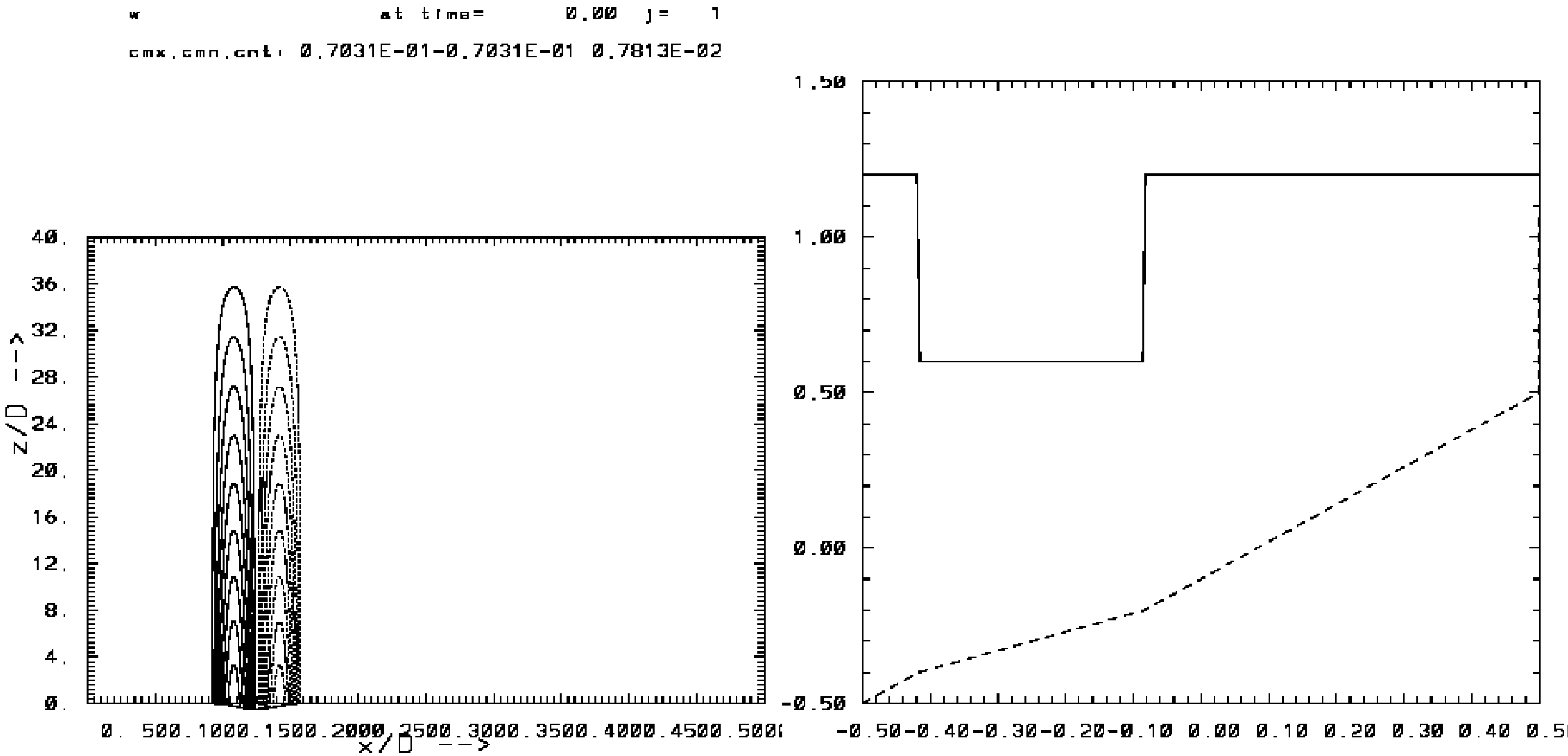
w at time= 0.00 j= 1
cmx,cmn,cnt: 0.7031E-01-0.7031E-01 0.7813E-02
z/D -->
x/D -->
0. 500. 1000. 1500. 2000. 2500. 3000. 3500. 4000. 4500. 5000
0. 4. 8. 12. 16. 20. 24. 28. 32. 36. 40.
-0.50 0.00 0.50 1.00 1.50
-0.50 -0.40 -0.30 -0.20 -0.10 0.00 0.10 0.20 0.30 0.40 0.50

Urban PBL (Smolarkiewicz et al. 2007, *JCP*) tests robustness of the continuous mapping approach

NCAR

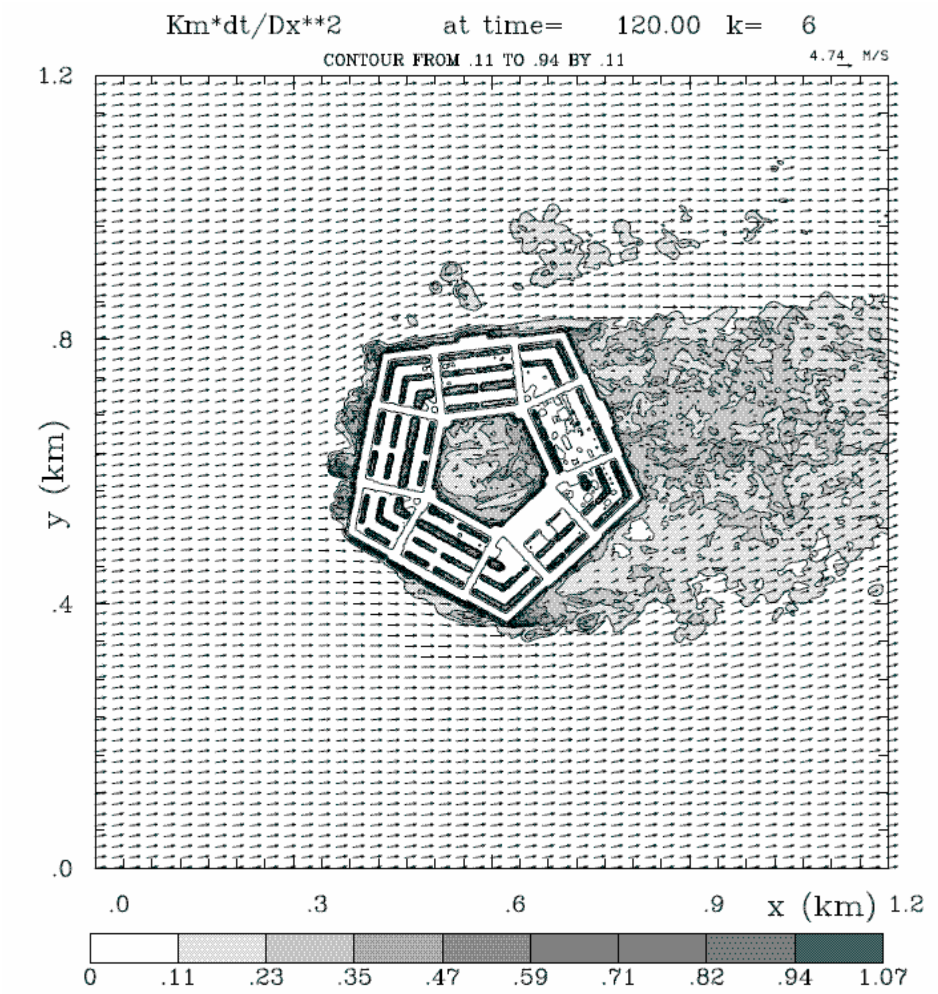

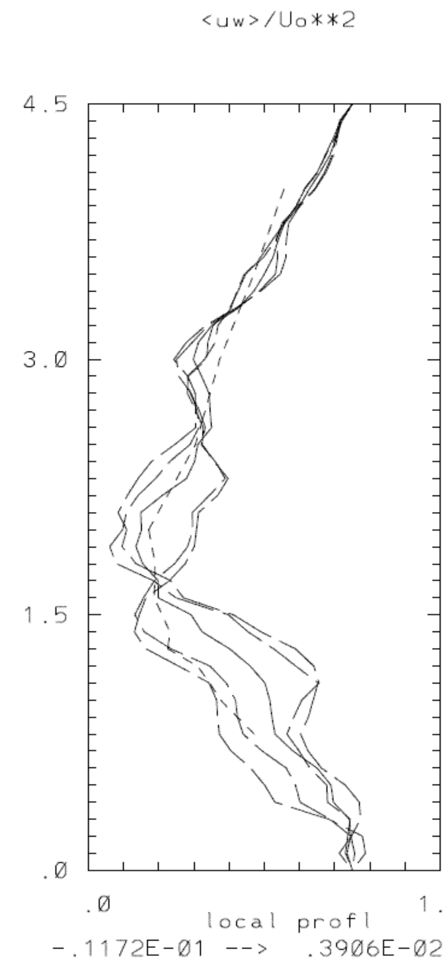

$\sqrt{TKE}$ contours in cross section at z=10 m

normalized profiles at a location in the wake $< u'w' >$

Model equations (intellectual kernel)

NCAR

Anelastic system of Lipps & Hemler (*JAS*, 1982)

$$\frac{\partial(\rho^* \overline{v^s}^k)}{\partial \overline{x}^k} = 0 \,. \tag{2}$$

$$\frac{dv^j}{d\overline{t}} = -\,\widetilde{G}^k_j \frac{\partial \pi'}{\partial \overline{x}^k} + g\frac{\theta'}{\theta_b}\delta_3{}^j + \mathcal{F}^j + \mathcal{V}^j \,, \tag{3}$$

$$\frac{d\theta'}{d\overline{t}} = -\overline{v^s}^k \frac{\partial \theta_e}{\partial \overline{x}^k} + \mathcal{H} \,, \tag{4}$$

$$\overline{v^s}^k := \overline{v^*}^k - \frac{\partial \overline{x}^k}{\partial t} \quad ; \quad \overline{v^s}^j = \widetilde{G}^j_k v^k \,. \tag{5}$$

$$\rho^* := \rho_b \overline{G} \quad ;$$

$$d/d\overline{t} = \partial/\partial\overline{t} + \overline{v^*}^k(\partial/\partial\overline{x}^k) \quad ;$$

$$\overline{v^*}^k := d\overline{x}^k/d\overline{t} := \dot{\overline{x}}^k$$

$$\widetilde{G}^k_j := \sqrt{g^{jj}}(\partial\overline{x}^k/\partial x^j) \quad \Leftarrow \quad ds^2 = g_{pq}dx^p dx^q \,,$$

$$g_{pk}g^{kq} \equiv \delta^q_p$$

$$\delta^r_s \equiv \frac{\partial \overline{x}^r}{\partial x^q}\frac{\partial x^q}{\partial \overline{x}^s}$$

$$\frac{G}{\overline{G}}\frac{\partial}{\partial \overline{x}^r}\left(\frac{\overline{G}}{G}\frac{\partial \overline{x}^r}{\partial x^s}\right) \equiv 0$$

NCAR

Strategies for simulating turbulent flows

- Direct numerical simulation (DNS), with all relevant scales of motion resolved, thus admitting variety of numerical methods;

- Large-eddy simulation (LES), with all relevant sub-grid scales parameterized, thus preferring higher-order methods;

- Implicit large-eddy simulation (ILES) — alias monotonically integrated large-eddy-simulation (MILES), or implicit turbulence modeling — with a bohemian attitude toward sub-grid scales and available only with selected numerical methods.

NCAR

DNS, with all relevant scales of motion resolved

- Important complement of laboratory studies, aiming at comprehension of fundamental physics, even though limited to low Reynolds number flows

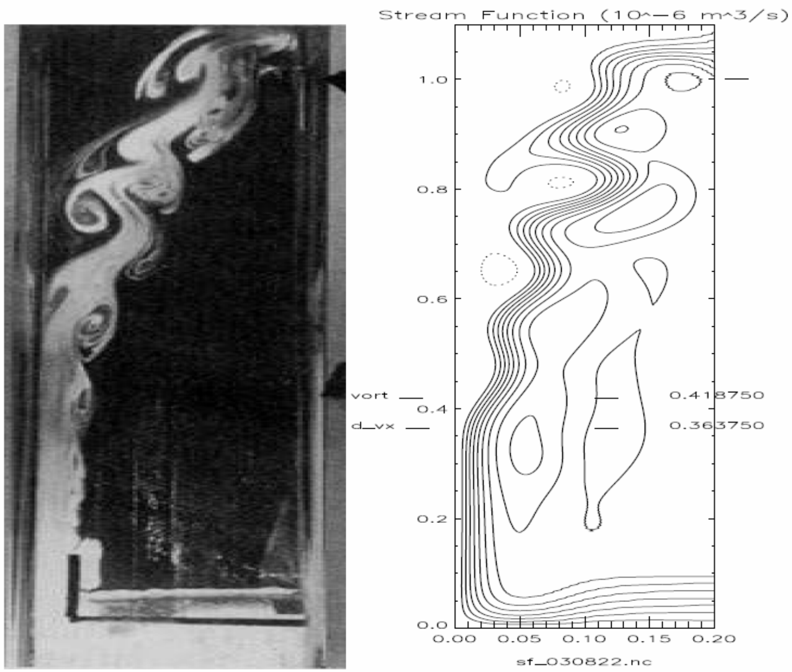

Figure 6: Baines & Hughes experiment (*JPO* 1996) vs. DNS

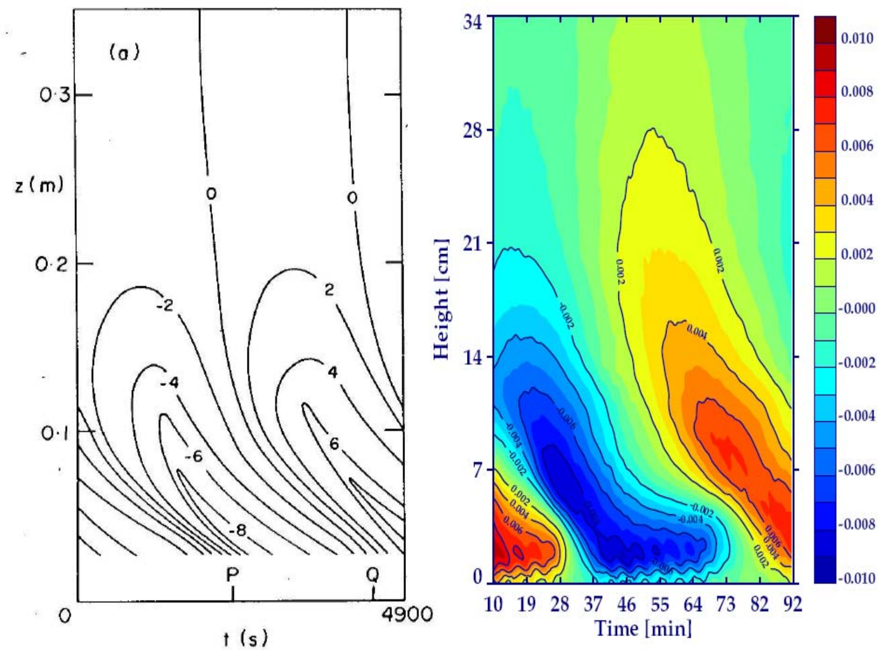

Figure 6: Time-height cross-section of the observed zonal-mean zonal flow velocity component (plate (a), adapted from Fig.10 in Plumb & McEwan (1978), contour lines are in mms^{-1}), compared to the result of the 3D numerical simulation at $y = L_y/2$ (plate (b), contour lines are in ms^{-1}). According to Plumb & McEwan (1978), the lowest 2 cm in plate (a) could not be observed due to restrictions of the viewing window; Nils Wedi, Ph.D thesis, +.

Plumb & McEvan (1978) lab experiment

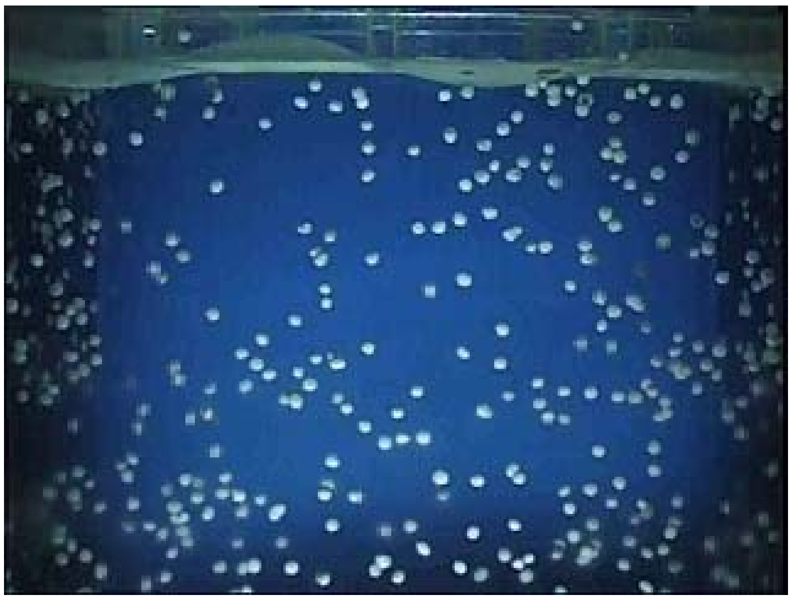

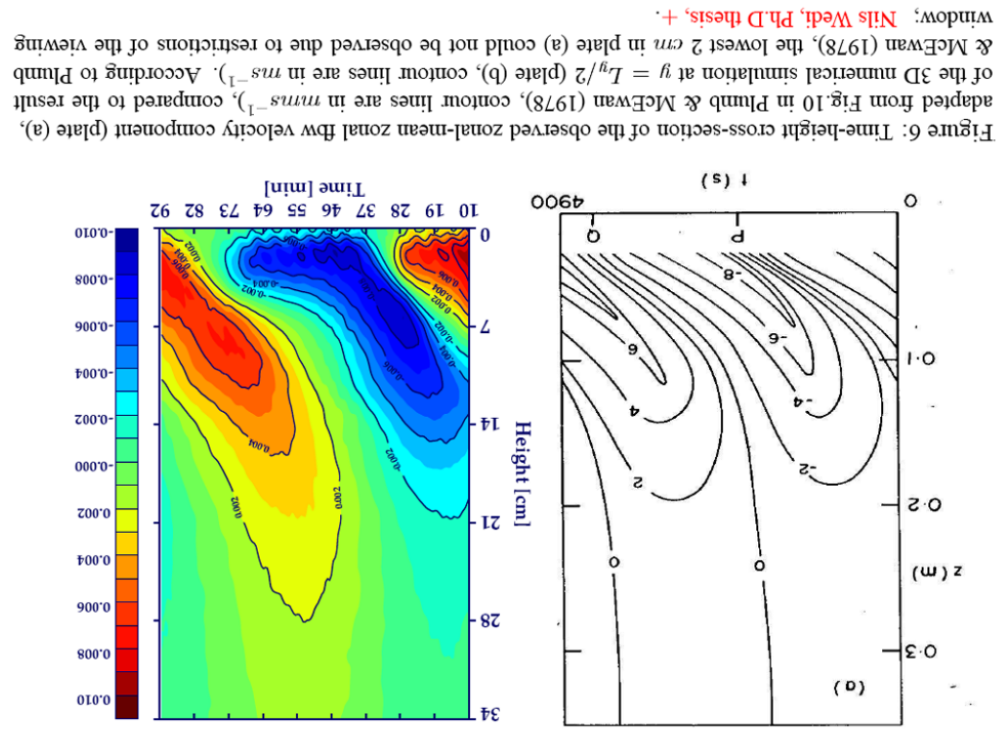

Analysis of the DNS results showed that the lab experiment is more relevant to the atmospheric QBO than appreciated (in the literature)

LES, with all relevant sub-grid scales parameterized

- Theoretical, physically-motivated SGS models lack universality and can be quite complicated in practice, yet they are effective (and thus important) for a range of flows; e.g., shear-driven boundary layers

Example: Simulations of boundary layer flows past rapidly evolving sand dunes

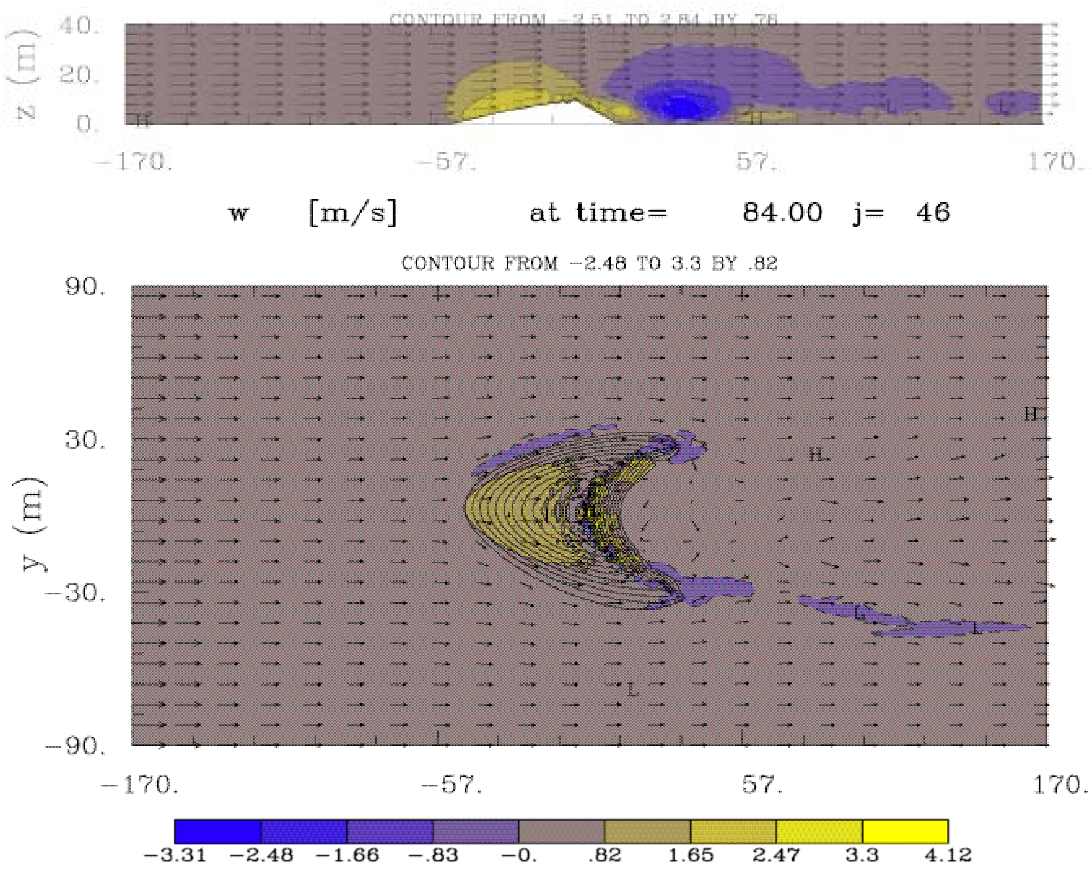

Domain 340x160x40 m^3 covered with dx=dy=2m dz=1m

Result depend on explicit SGS model (here TKE), because the saltation physics that controls dunes' evolution depends crucially on the boundary stress.

LES, with all relevant sub-grid scales parameterized

NCAR

- Theoretical, physically-motivated SGS models lack universality and can be quite complicated in practice; yet they are effective, and thus important, for shear-driven boundary layer flows

Example: Simulations of boundary layer flows past sand dunes

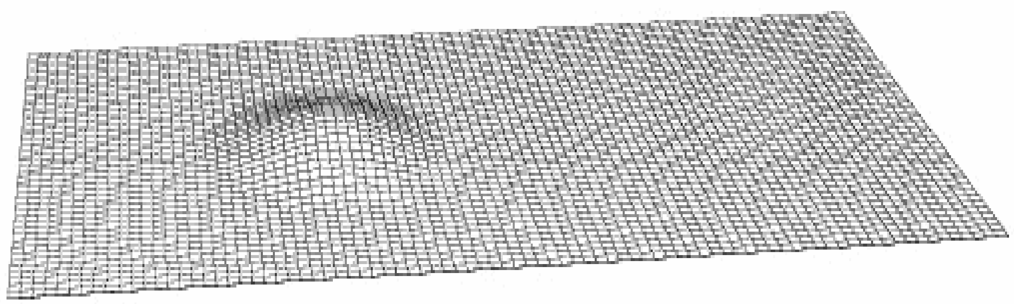

Domain 340x160x40 m^3 covered with dx=dy=2m dz=1m

Results depend on explicit SGS model (here TKE), because the saltation physics that controls dunes' evolution depends crucially on the boundary stress.

LES vs RANS; urban PBL (Smolarkiewicz et al.2007,*JCP*)

NCAR

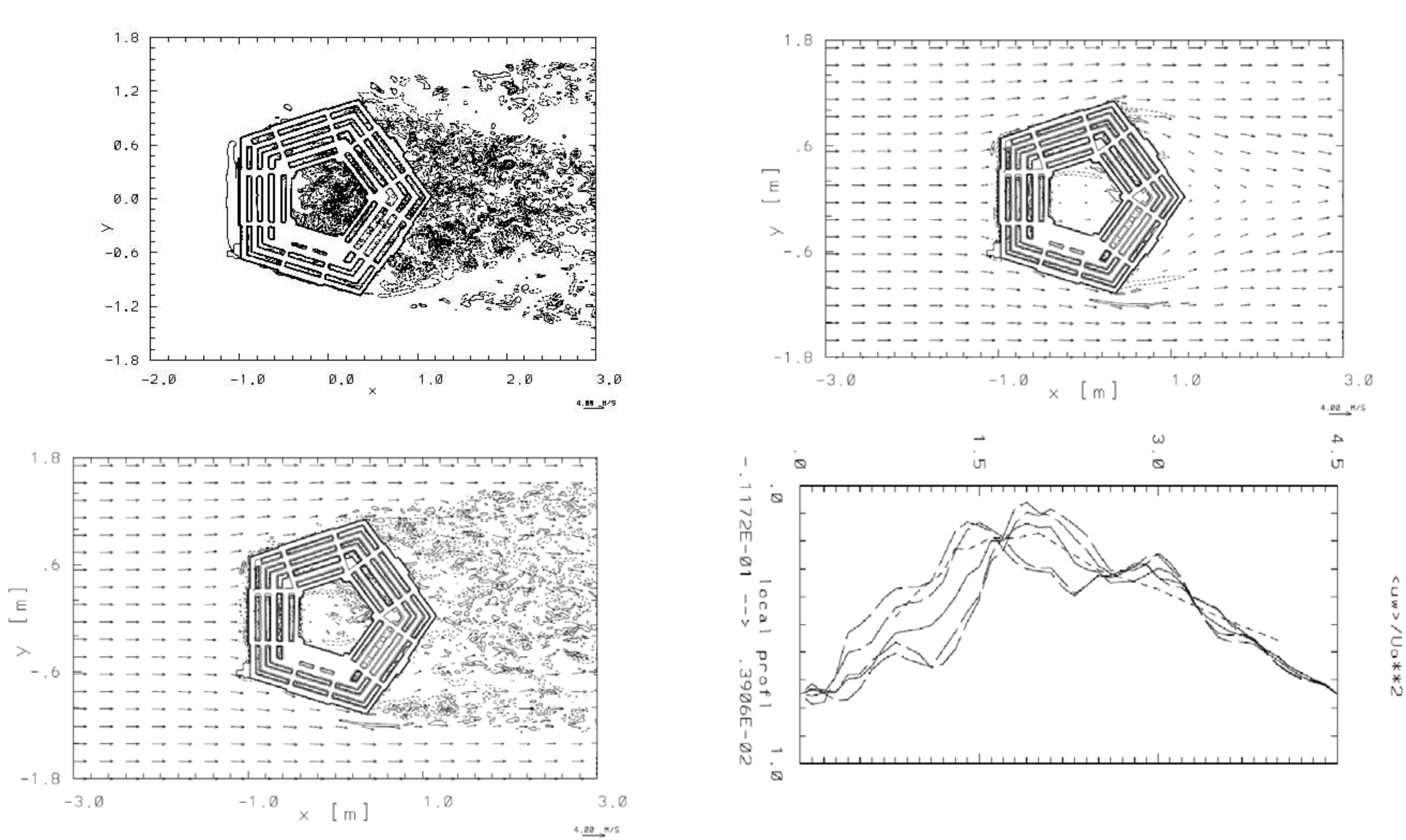

LES/ILES of convective PBL, after Margolin et al. 1999.

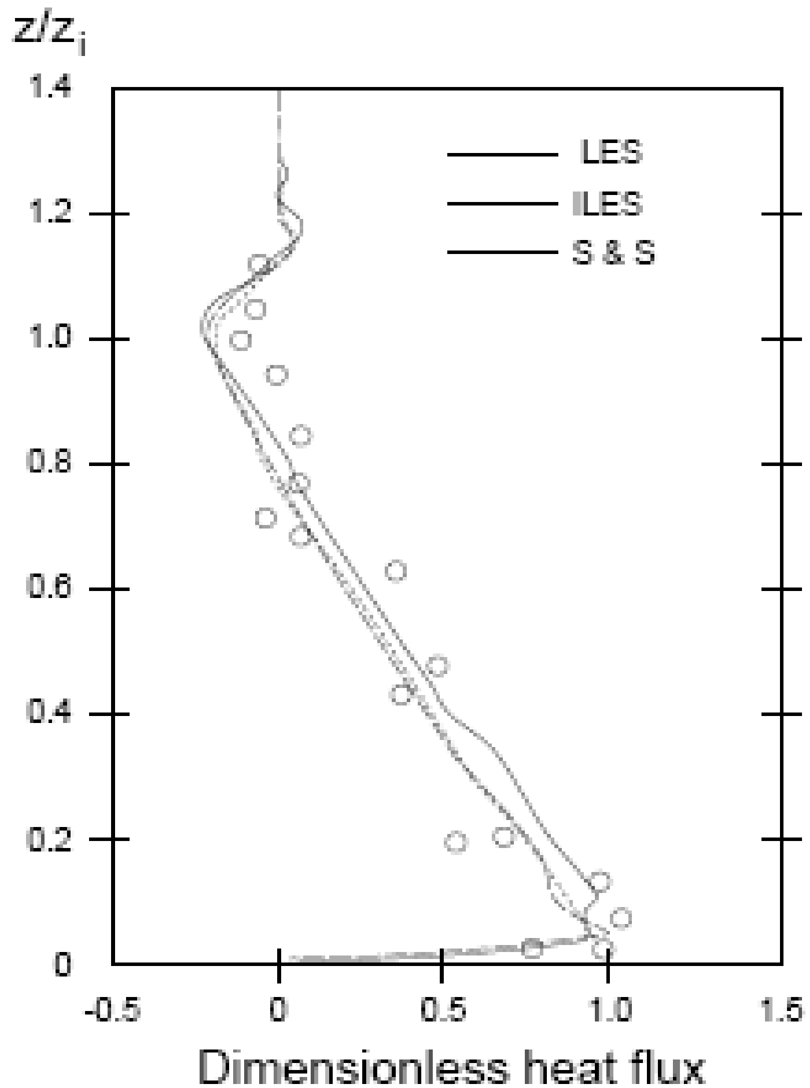

NCAR

ILES:

- Controversial approach, yet theoretically sound and practical, thus gaining wide appreciation

- Cumulative experience of the community covers broad range of flows and physics; *Implicit Large Eddy Simulation: Computing Turbulent Fluid Dynamics.* Ed. Grinstein FF, Margolin L, and Rider W. Cambridge University Press, 2007

- The EULAG's experience includes rotating stratified flows on scales from laboratory to global circulations and climate.

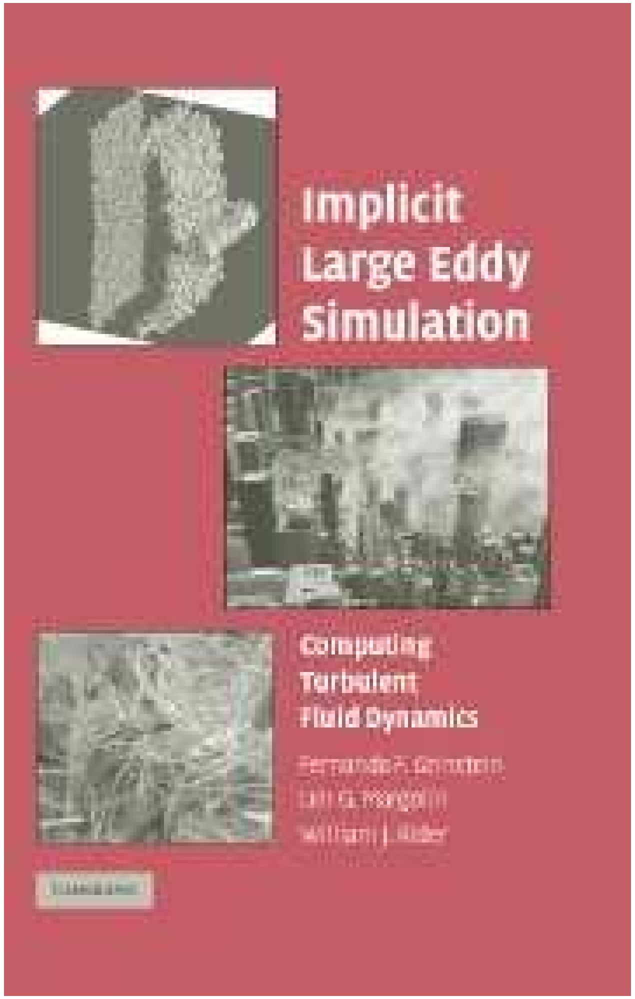

Canonical decaying-turbulence studies demonstrate the soundness of the approach

NCAR

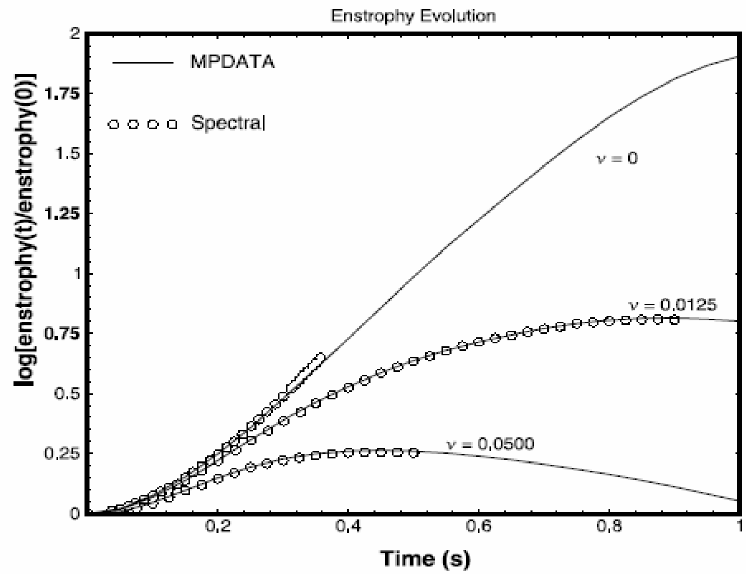

Figure 3: 256^3 DNS/ILES of transient decaying turbulence; Margolin et al. *J. Fluid Eng.* 2002.

time	1.00	1.25	1.50	1.75	2.00
$-15 < u_x^3 > \delta x^2/(4\varepsilon)$	0.785	0.933	1.028	1.054	1.019

Table 1: Verification of "4/5" Kolmogorov's law $\langle(\delta v_{\,||}(\mathbf{r},\mathbf{l}))^3\rangle = -\frac{4}{5}\varepsilon l \quad \Rightarrow \quad \varepsilon \sim v_o^3/l_o$; $\delta v_{||}(\mathbf{r},\mathbf{l}) := [\mathbf{v}(\mathbf{r}+\mathbf{l}) - \mathbf{v}(\mathbf{r})]\cdot(\mathbf{l}/l)$, $\quad v_o := \sqrt{\langle \mathbf{v}(\mathbf{r}+\mathbf{l}_o)\cdot\mathbf{v}(\mathbf{r})\rangle}$ — Frisch 1995.

NCAR

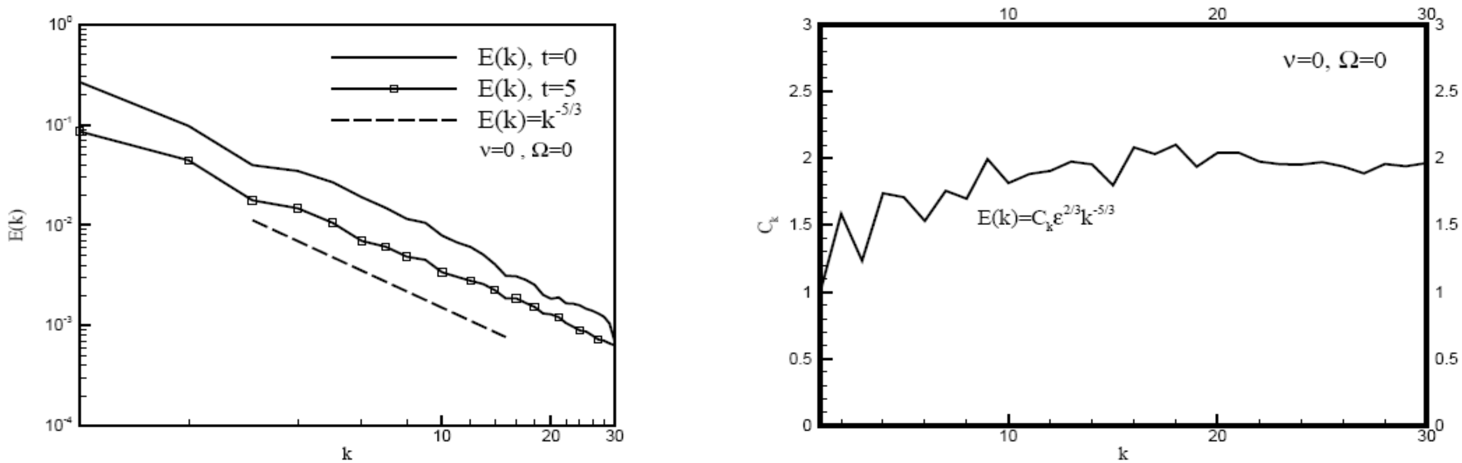

Figure 4: 64^3 ILES of decaying turbulence, Domaradzki et al. *Phys. Fluids* 2003. Energy spectra and Kolmogorov function $C_K(k) = \varepsilon^{-2/3}k^{5/3}E(k)$ dla $\nu = 0.0$ $\Leftrightarrow \ \langle(\delta v_{||}(l))^2\rangle \sim l^{2/3}$

$$\frac{\partial E(k,t)}{\partial t} = T(k,t) - 2\nu k^2 E(k) - \varepsilon_n(k,t) \Rightarrow \varepsilon_n := 2\nu_n k^2 E(k) \Rightarrow \nu_n(k)$$

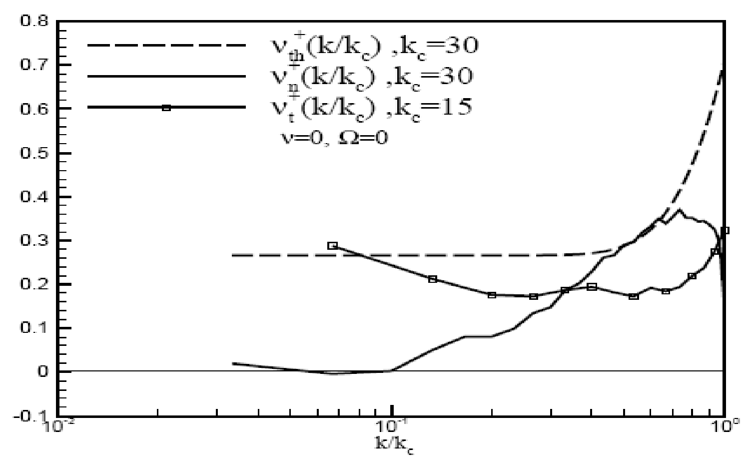

NCAR

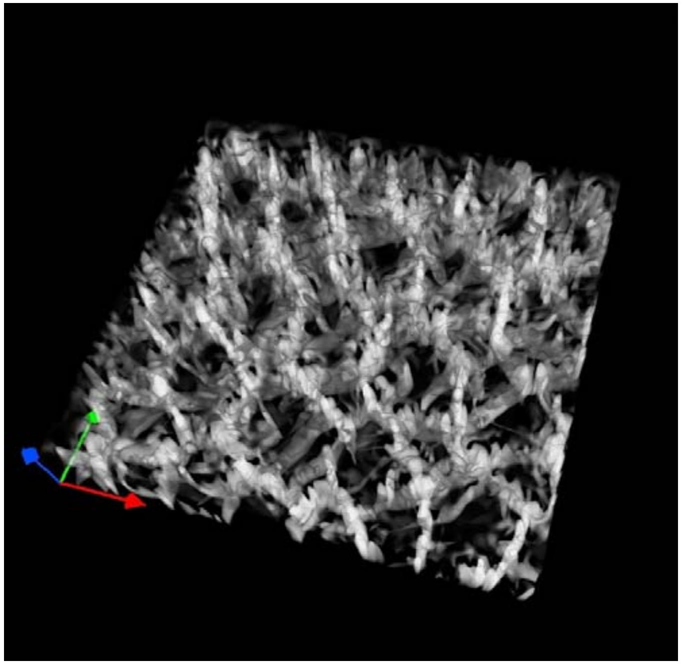

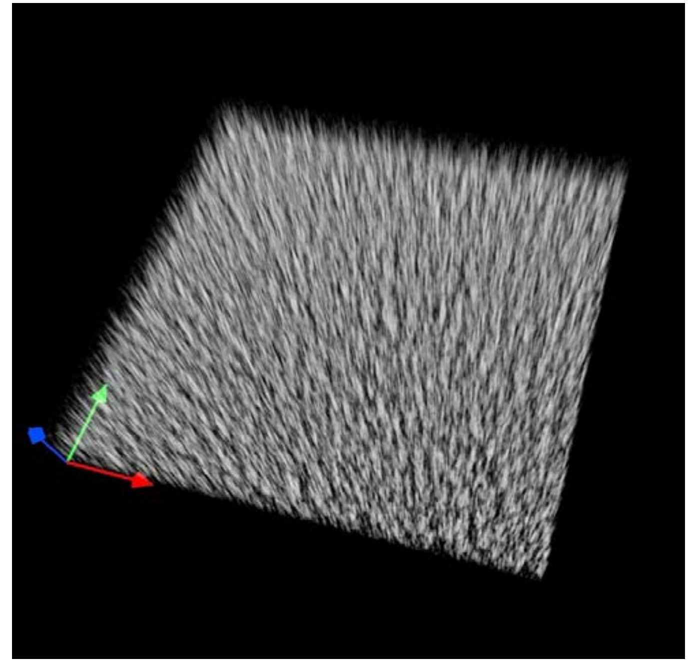

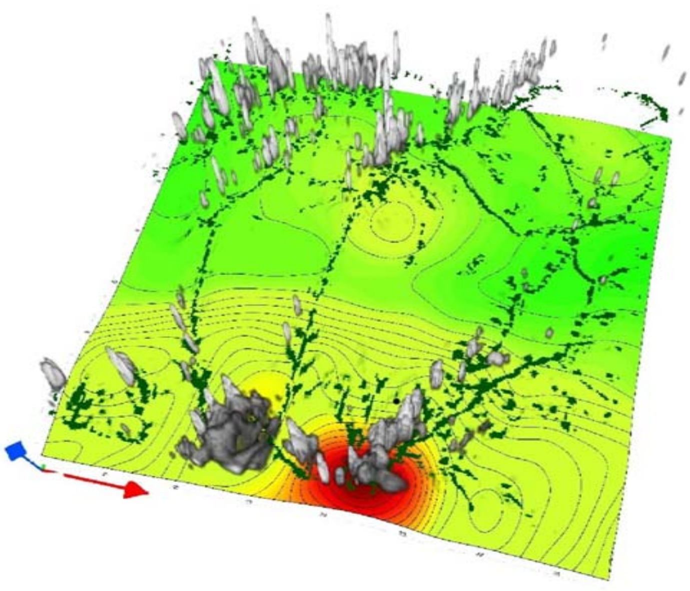

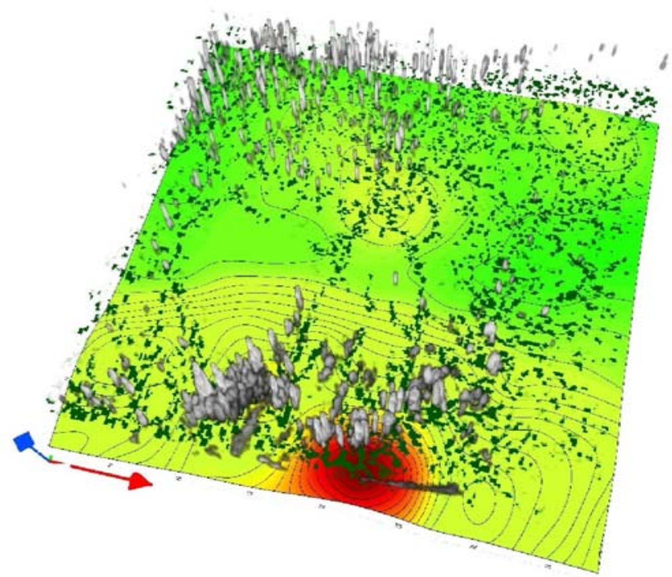

Global circulation and climate

NCAR

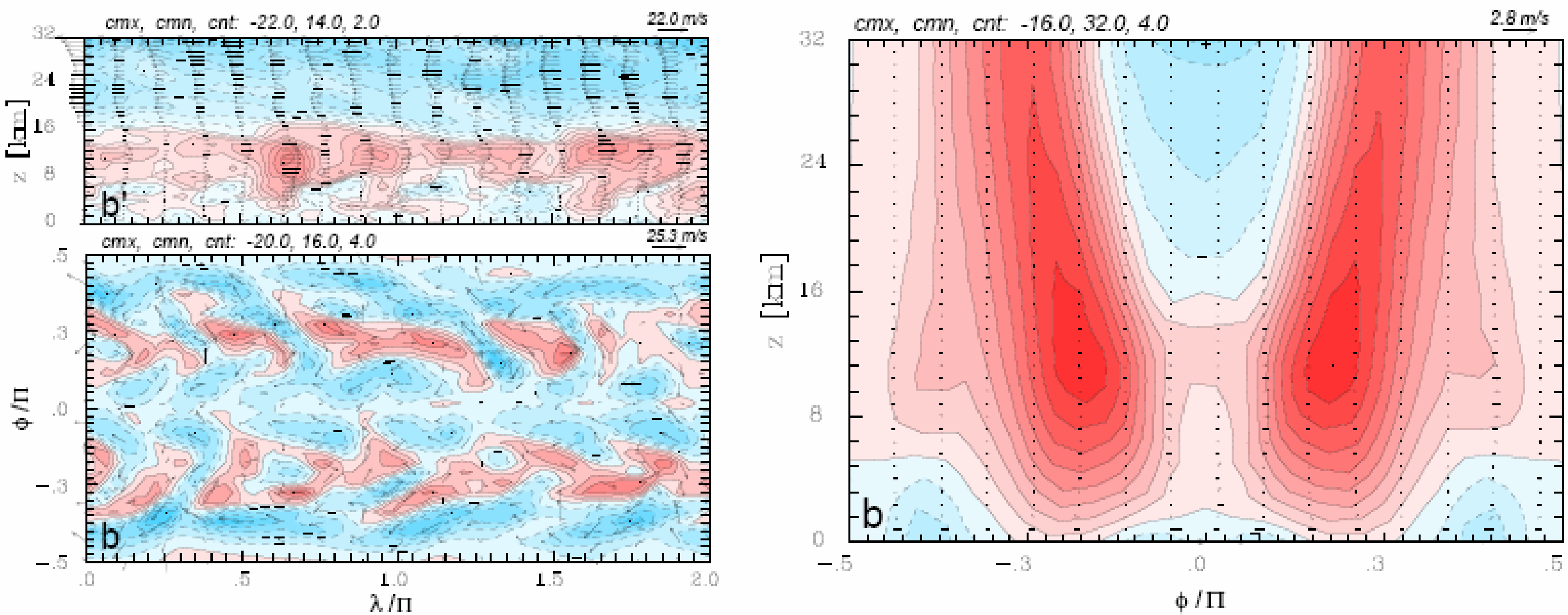

Figure 2: The idealized Held-Suarez climate problem (*BAMS* 1994); instantaneous solution after 3 years of simulation (left), and zonally averaged 3-year means (right) (Sm. et al. *JAS* 2001).

DNS / ILES

NCAR

Example: Solar convection (Elliott & Smolarkiewicz, 2002)

Deep convection in the outer interior of the Sun

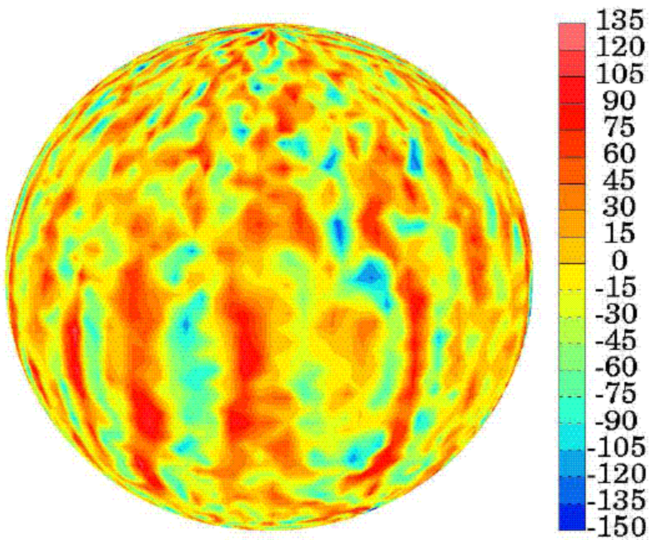

vertical velocity [ms−1] on a horizontal surface near the middle of the domain for the ILES run

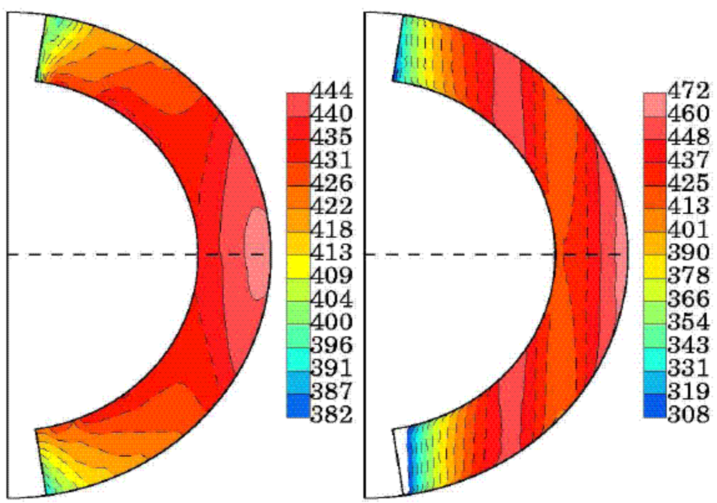

DNS ILES

time-averaged angular velocity [nHz]

- Both simulations produced similar patterns of vertical velocity, with banana-cell convective rolls and velocities of the order of a few hundred [m/s]
- DNS and the ILES solutions produced similar patterns of mean meridional circulation, but differed in predicting the pattern of the differential rotation

NCAR

Recent extensions, MHD

$$\nabla \cdot (\rho_s \mathbf{v}) = 0,$$

$$\frac{D\mathbf{v}}{Dt} = -\nabla\left(\frac{p'}{\rho_s} + \frac{\mathbf{B}^2}{2\mu\rho_s}\right) - \mathbf{g}(\mathbf{r})\frac{\theta'}{\theta_s} + 2\mathbf{v}' \times \boldsymbol{\Omega} + \frac{1}{\mu\rho_s}(\mathbf{B}\cdot\nabla)\,\mathbf{B} - \frac{1}{\rho_s}\nabla\cdot\boldsymbol{\tau},$$

$$\frac{D\theta'}{Dt} = -\mathbf{v}\cdot\nabla\theta_e + \underbrace{\frac{\theta_s}{c_p\rho_s T_s}\varepsilon}_{\text{radiation}} + \underbrace{\frac{1}{\rho_s}\nabla\cdot(\kappa\rho_s\nabla\theta')}_{\text{diffusion}} + \underbrace{\frac{\theta_s}{c_p\rho_s T_s}\mathbf{v}\cdot(\nabla\cdot\boldsymbol{\tau})}_{\text{viscous heating}},$$

$$\frac{D\mathbf{B}}{Dt} = (\mathbf{B}\cdot\nabla)\,\mathbf{v} - \mathbf{B}(\nabla\cdot\mathbf{v}) + \eta\nabla^2\mathbf{B}, \quad \nabla\cdot\mathbf{B} = \mathbf{0},$$

Governing Equations: terrestrial-object-oriented form

$$\nabla \cdot (\rho_s \mathbf{v}) = 0, \tag{5}$$

$$\frac{D\mathbf{v}}{Dt} = -\nabla\phi - \mathbf{g}(\mathbf{r})\frac{\theta'}{\theta_s} - \mathbf{f} \times \mathbf{v}' + \frac{1}{\mu\rho_s}(\mathrm{B} \cdot \nabla)\,\mathrm{B} + \mathcal{D}_{\mathbf{v}} \tag{6}$$

$$\frac{D\theta'}{Dt} = -\mathbf{v} \cdot \nabla\theta_e + \mathcal{H} \tag{7}$$

$$\frac{D\mathrm{B}}{Dt} = -\nabla\phi^* + (\mathrm{B} \cdot \nabla)\,\mathbf{v} - \mathrm{B}(\nabla \cdot \mathbf{v}) + \mathcal{D}_{\mathrm{B}} \;\; ; \quad \nabla \cdot \mathrm{B} = \mathbf{0} \tag{8}$$

Note: Analytically, $\nabla\phi^* \equiv 0$ and $(\mathrm{B} \cdot \nabla)\,v^I \equiv \nabla \cdot \left(\mathrm{B}v^I\right)$.

Approximate Integrals

NCAR

$$\psi_{\mathrm{i}}^{n+1} = \mathcal{A}_{\mathrm{i}}(\psi^n + 0.5\delta t R^n) + 0.5\delta t R_{\mathrm{i}}^{n+1} \;\equiv\; \widehat{\psi}_{\mathrm{i}} + 0.5\delta t R_{\mathrm{i}}^{n+1}; \qquad (9)$$

• (9) is implicit for all dependent variables in (6)-(8). To retain this proven structure for the MHD system, (9) is executed in the spirit of

$$\Psi_{\mathrm{i}}^{n+1,\nu} = \widehat{\Psi}_{\mathrm{i}} + 0.5\delta t\, \mathbf{L}\Psi\big|_{\mathrm{i}}^{n+1,\nu} + 0.5\delta t\, \mathbf{N}\Psi\big|_{\mathrm{i}}^{n+1,\nu-1} - \nabla\Phi\big|_{\mathrm{i}}^{n+1,\nu} \;\Longrightarrow \qquad (10)$$

$$\Psi_{\mathrm{i}}^{n+1,\nu} = \left[\mathbf{I} - 0.5\delta t\, \mathbf{L}\right]^{-1} \left(\widehat{\Psi} + 0.5\delta t\, \mathbf{N}\Psi\big|^{n+1,\nu-1} - \nabla\Phi^{n+1,\nu}\right)\Big|_{\mathrm{i}} \qquad (11)$$

where $\mathbf{L}$ and $\mathbf{N}$ denote linar and nonlinear part of the rhs R, $\Psi \equiv (\mathrm{v},\ \theta',\ \mathrm{B})$, $\Phi \equiv 0.5\delta t(\phi,\ \phi,\ \phi,\ 0,\ \phi^*,\ \phi^*,\ \phi^*)$, and $\nu = 1, .., m$ numbers the iterations.

- In particular:

$$\mathbf{B}_{\mathbf{i}}^{n+1,\nu-1/2} = \widehat{\mathbf{B}}_{\mathbf{i}} + 0.5\delta t\left[(\mathbf{B}^{n+1,\nu-1/2}\cdot\nabla)\mathbf{v}^{n+1,\nu-1} - \mathbf{B}^{n+1,\nu-1/2}(\nabla\cdot\mathbf{v}^{n+1,\nu-1})\right]_{\mathbf{i}}\ ; \tag{12}$$

$$\begin{aligned}
\theta'|_{\mathbf{i}}^{n+1,\nu} &= \widehat{\theta'}_{\mathbf{i}} - 0.5\delta t\left(\mathbf{v}^{n+1,\nu}\cdot\nabla\theta_e\right)_{\mathbf{i}}\ , \\
\mathbf{v}_{\mathbf{i}}^{n+1,\nu} &= \widehat{\mathbf{v}}_{\mathbf{i}} + \frac{0.5\delta t}{\mu\rho_s}(\mathbf{B}\cdot\nabla\mathbf{B})_{\mathbf{i}}^{n+1,\nu-1/2} \\
&\quad -0.5\delta t\left[\nabla\phi|^{n+1,\nu} + \mathbf{g}\frac{\theta'|^{n+1,\nu}}{\theta_s} + \mathbf{f}\times(\mathbf{v}^{n+1,\nu}-\mathbf{v}_e)\right]_{\mathbf{i}}\ , \\
\nabla\cdot(\rho_s\mathbf{v}^{n+1,\nu}) &= 0\ ,
\end{aligned} \tag{13}$$

solve for $\phi^{n+1,\nu}$, $\mathbf{v}^{n+1,\nu}$ and $\theta'|^{n+1,\nu}$ via elliptic problem for $\phi^{n+1,\nu}$;

$$\mathbf{B}_{\mathbf{i}}^{n+1,\nu-3/4} = \widehat{\mathbf{B}}_{\mathbf{i}} + 0.5\delta t\left[(\mathbf{B}^{n+1,\nu-3/4}\cdot\nabla)\mathbf{v}^{n+1,\nu} - \mathbf{B}^{n+1,\nu-3/4}(\nabla\cdot\mathbf{v}^{n+1,\nu})\right]_{\mathbf{i}}\ ; \tag{14}$$

$$\begin{aligned}
\mathbf{B}_{\mathbf{i}}^{n+1,\nu} &= \widehat{\mathbf{B}}_{\mathbf{i}} + 0.5\delta t\left[(\mathbf{B}^{n+1,\nu-3/4}\cdot\nabla)\mathbf{v}^{n+1,\nu} - \mathbf{B}^{n+1,\nu-3/4}(\nabla\cdot\mathbf{v}^{n+1,\nu})\right]_{\mathbf{i}} \\
&\quad -0.5\delta t\nabla\phi^*|^{n+1,\nu}\ , \\
\nabla\cdot\mathbf{B}^{n+1,\nu} &= 0\ ,
\end{aligned} \tag{15}$$

solve for $\phi^*|^{n+1,\nu}$ and $\mathbf{B}^{n+1,\nu}$ via elliptic problem for $\phi^*|^{n+1,\nu}$.

Results: HD versus MHD convection, 100 $\odot$days

NCAR

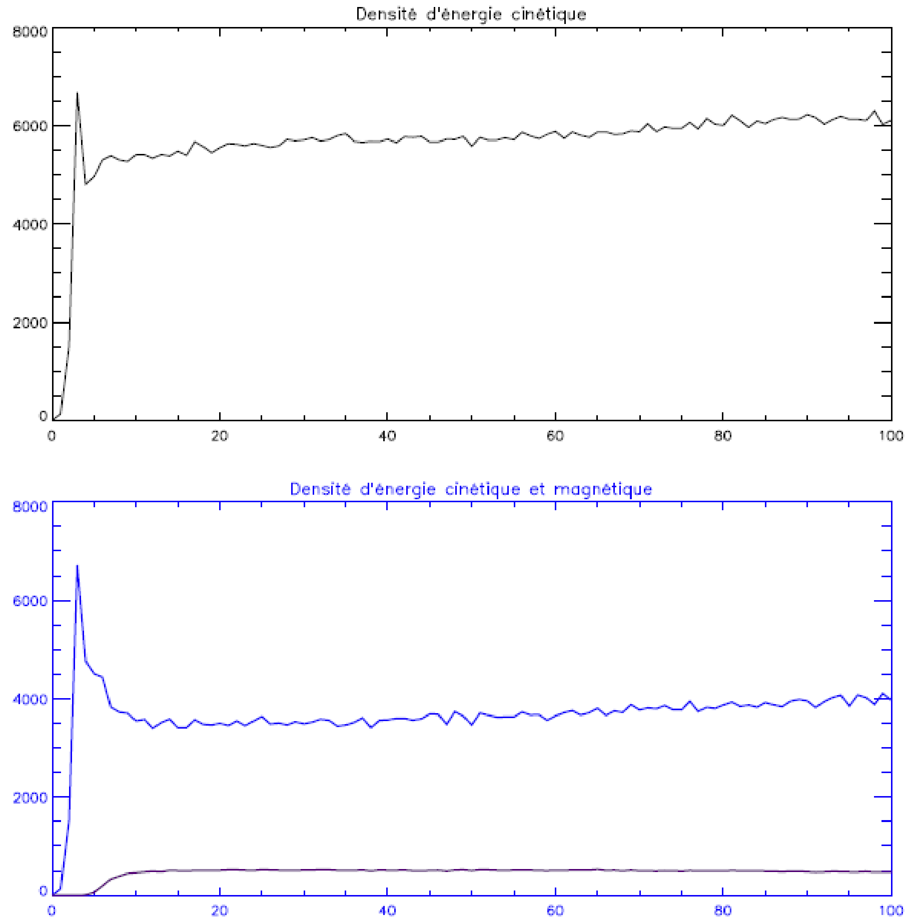

Figure 2: Kinetic $\langle \rho_s \mathbf{v}^2/2 \rangle$ and magnetic $\langle \mathrm{B}^2/(2\mu) \rangle$ energy, HD vs MHD run.

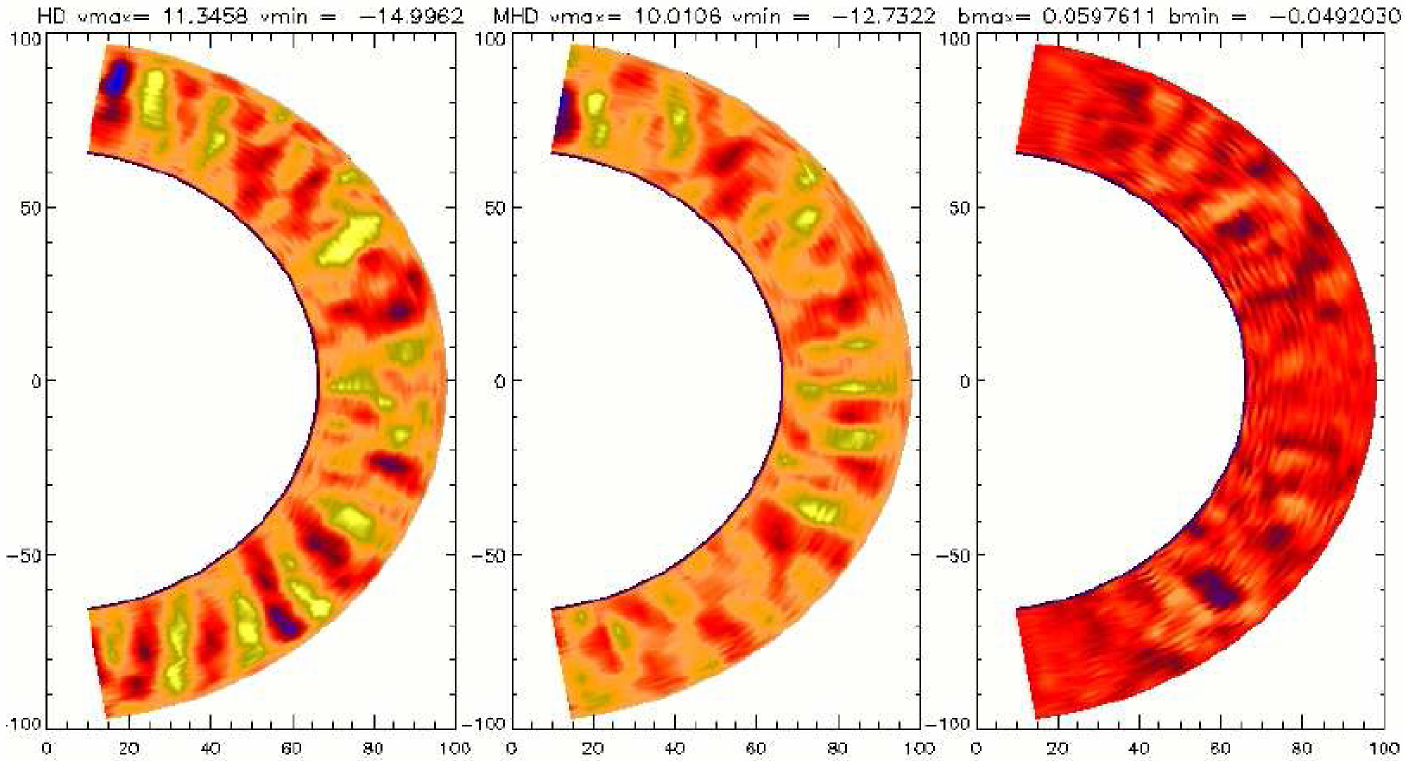

Figure 4: w and B_z field in latitude-radius projection.

NCAR

Other extensions include the Durran and compressible Euler equations.
Designing principles are always the same:

$$\frac{\partial \mathbf{\Phi}}{\partial t} + \nabla \bullet (\mathbf{V}\mathbf{\Phi}) = \mathbf{R} \ ,$$

$$\forall_i \quad \mathbf{\Phi}_i^{n+1} = \mathbf{\Phi}_i^{*} + 0.5\delta t \mathbf{R}_i^{n+1} \qquad \mathbf{\Phi}^{*} \equiv \mathcal{A}(\mathbf{\Phi}^{n} + 0.5\delta t \mathbf{R}^{n}, \widehat{\mathbf{V}}^{n+1/2})$$

$$\forall_i \quad \mathbf{\Phi}_i^{n+1,\ \mu} = \mathbf{\Phi}_i^{*} + 0.5\delta t \mathbf{R}_i^{n+1,\ \mu-1}$$

$$\begin{aligned} \|\ \mathbf{\Phi}^{n+1,\ \mu} - \mathbf{\Phi}^{n+1}\ \| \ &= \ 0.5\delta t\ \|\ \mathrm{R}(\mathbf{\Phi}^{n+1,\ \mu-1}) - \mathrm{R}(\mathbf{\Phi}^{n+1})\ \| \\ &\leq 0.5\delta t\ \sup\ \|\ \partial \mathrm{R}/\partial \mathbf{\Phi}\ \|\|\ \mathbf{\Phi}^{n+1,\ \mu-1} - \mathbf{\Phi}^{n+1}\ \| \end{aligned}$$

Remarks

NCAR

Synergetic interaction between
- (i) rules of continuous mapping (e.g., tensor identities),
- (ii) strengths of nonoscillatory forward-in-time (NFT) schemes,
- (iii) virtues of the anelastic formulation of the governing equations

facilitates design of robust multi-scale multi-physics models for geophysical flows.

The direct numerical simulation (DNS), large-eddy simulation (LES), and implicit large-eddy simulation (ILES) turbulence modeling capabilities, facilitate applications at broad range of Reynolds numbers (Smolarkiewicz and Prusa 2002 → Smolarkiewicz and Margolin, 2007).

Parallel performance was never an issue. The code was shown to scale from O(10) up to 16000 processors. The satisfactory parallel performance is a total of selected numerical methods (NFT MPDATA based + Krylov elliptic solvers) and hard-coded parallel communications throughout the code; i.e., no user-friendly interface!